# Waves and bumps in neuronal networks with axo-dendritic synaptic interactions

S Coombes[†], G J Lord[‡] and M R Owen[†]

[†]*Department of Mathematical Sciences, Loughborough University, Loughborough, Leics., LE11 3TU, UK.*

[‡]*Department of Mathematics, Heriot-Watt University, Edinburgh, EH14 4AS, UK*

**Abstract**

We consider a firing rate model of a neuronal network continuum that incorporates axo-dendritic synaptic processing and the finite conduction velocities of action potentials. The model equation is an integral one defined on a spatially extended domain. Apart from a spatial integral mixing the network connectivity function with space-dependent delays, arising from non-instantaneous axonal communication, the integral model also includes a temporal integration over some appropriately identified distributed delay kernel. These distributed delay kernels are biologically motivated and represent the response of biological synapses to spiking inputs. They are interpreted as Green's functions of some linear differential operator. Exploiting this Green's function description we discuss formal reductions of this non-local system to equivalent partial differential equation (PDE) models. We distinguish between those spatial connectivity functions that give rise to local PDE models and those that give rise to PDE models that require both advanced and retarded terms. For cases in which local PDEs are derived, we investigate traveling wave solutions in a comoving frame by numerically computing global heteroclinic connections. We then calculate exact solutions, parameterized by axonal conduction velocity, for sigmoidal firing rate functions in the limit of infinite gain, for a variety of spatial connectivities and synaptic responses. The inclusion of synaptic adaptation is shown to alter traveling wave fronts to traveling pulses, which we study analytically and numerically in terms of a global homoclinic orbit. Finally, we consider the impact of dendritic interactions on waves and on static spatially localized solutions. Exact analysis for

infinite gain shows that axonal delays do not affect the stability of single bumps. Furthermore, numerical continuation for finite gain leads to multiple bump solutions, and it is demonstrated that such localized multi-bumps are lost (in favor of global patterns) when a stable $N$-bump and an unstable $(N+2)$-bump coalesce. In essence, the work in this paper illustrates how physiologically significant features of synaptic processing, synaptic adaptation and patterns of axo-dendritic connectivity may be analyzed within a neural field firing rate framework.

*Key words:* neuronal networks, integral equations, space dependent delays, traveling waves, patterns, axo-dendritic synapses, Hamiltonian fourth order systems.

---

## 1 Introduction

Traveling waves in neurobiology are receiving increased attention by experimentalists, in part due to their ability to visualize them with multi-electrode recordings and imaging methods. In particular it is possible to electrically stimulate slices of pharmacologically treated tissue taken from the cortex [1], hippocampus [2] and thalamus [3] and also living spinal preparations of simple vertebrates [4]. Under a variety of circumstances this results in the propagation of electrical activity in the form of a traveling wave. In brain slices these waves can take the form of spindle waves seen at the onset of sleep, the propagation of synchronous discharge during an epileptic seizure [5] and waves of excitation associated with sensory processing [6]. In vertebrates the waves of activity observed in the spinal cord are generators for locomotor patterns. Experiments in primates have also revealed that prefrontal cortical networks can support spatially localized areas of high activity, thought to be important for the functioning of working memory [7]. Such waves and bumps of firing rate activity are a consequence of non-local synaptic interactions and the intrinsic behavior of local neuronal circuitry.

Many cells in nature are excitable in the sense that a sufficiently strong stimulus will induce the membrane potential of the cell to undergo a large excursion, known as an action potential, before coming back to rest. Action potentials generated at the axon hillock travel along axons, via the regenerative movement of ions across the cell membrane, and terminate at synapses on postsynaptic dendrites. Here they produce potentials that accumulate to trigger (or inhibit) further action potentials. The mean firing rate for single neuron action potential generation is a natural variable for describing traveling waves and spatially localized bumps of neural activity at the network level. The class of computational models that are believed to support synaptic waves and bumps differ radically from classic models of waves in excitable systems. Most importantly, synaptic interactions are non-local (in space), involve communication (space-dependent) delays (arising from the finite propagation velocity of an action potential) and distributed delays (arising from neurotransmitter release and dendritic processing). In contrast many studies of excitable waves assume that the underlying mechanism for wave propagation is diffusive in nature, as exemplified by an action potential traveling along an axon. The strong and growing body of experimental data relating to the anatomy, electro-physiology and pharmacology of brain slice preparations has encouraged the development of detailed biophysical models. Numerical simulations of these models have shown that the broad

features associated with wave propagation have been captured (see for example [1, 8, 9]). For thalamic slice models these include the generation of both spontaneous and evoked spindle episodes, the high degree of synchrony between neuronal sub-populations and the observation of traveling fronts with speeds around 1 mm/s (60-90 mm/s for cortical slices). An inherent problem with this approach is the analytically intractable nature of such detailed models and that large scale network simulations are computationally expensive with many adjustable parameters. To help redress the balance between simulation results and mathematical analysis we present our study of a minimal model neuronal network with biologically motivated forms of axo-dendritic synaptic interaction. Moreover, we explicitly show how to analyze the effects of dendritic processing and axonal communication delays commonly neglected in mathematical studies.

In Section 2 we introduce an integral equation model which describes the firing rate of a population of neurons in terms of their connectivity and synaptic processing, subject to delays due to the finite speed of axonal signal propagation. We then exploit the language of Green's functions in Section 3 to determine equivalent PDE models. In Section 4 we change to a comoving frame and focus on traveling wave solutions. For Heaviside firing rate functions we calculate the speed of propagation of traveling fronts exactly. Numerical shooting and continuation is used to explore the properties of solutions that arise for more general sigmoidal shaped firing rate functions. Our work builds upon that of Pinto and Ermentrout [10] and is illustrated for various popular choices of synaptic response and connectivity. A form of spike frequency adaptation, similar to that in [10], is presented in Section 5. The model is shown to be exactly soluble for Heaviside firing rate functions allowing the explicit construction of traveling pulses. In Section 6 we extend our study to include dendritic processing and discuss biophysically realistic choices of axo-dendritic connectivity that reduce our original integral model to a well known reaction diffusion system. The inclusion of dendritic interactions is also shown to significantly influence the properties of time independent solutions. In Section 7 we discuss the forms of axo-dendritic connectivity that give rise to spatially localized solutions. Such solutions of non-local neural field theories have recently been linked by Laing *et al.* [11] to corresponding solutions of an associated fourth order Hamiltonian system. Motivated by this work we present an analysis of the Hamiltonian system associated with the integral model arising in the presence of passive dendrites. The stability of localized solutions is formulated as an eigenvalue problem, which we solve exactly for single bump solutions, along the lines described in [12]. Finally in Section 8 we summarize the major points of this paper and

discuss natural extensions of our work.

## 2 Integral equation model

Biophysical models of single (point) neurons often have the following form:

$$C\frac{\mathrm{d}V}{\mathrm{d}t} = -\sum_k g_k m_k^{p_k} h_k^{q_k}(V - V_k) + u, \tag{1}$$

where $p_k, q_k \in \mathbb{Z}$, $m_k$ and $h_k$ are gating variables that satisfy differential equations, $V_k$ is the reversal potential of the $k$th channel, $g_k$ are a set of constants, and $u$ is an applied current. When the gating variables are described by the Hodgkin-Huxley model, positive feedback may result in the generation of an action-potential or spike of voltage. The voltage generally comes back down due to two effects: (i) turning on of outward currents and (ii) inactivation of the inward currents. Thus, application of a constant current causes the neuron to spike, repolarize, and spike again. The steady rate of firing that occurs in the presence of a constant current results in the so-called firing rate function which plays a major role in many neural network models. Appropriate choices for the number and type of conductance channels and their associated gating variables can lead to other types of neural firing patterns such as bursting (see [13] for a discussion of voltage gated models which gives explicit formulae for many different channels and gates that are found in thalamic and cortical neurons). In many continuum models for the propagation of electrical activity in neural tissue it is assumed that the synaptic input current is a function of the pre-synaptic firing rate function [14, 15, 16, 17]. To see how this might arise consider a one-dimensional continuum of spiking single neurons with synaptic input at position $x$ given by

$$u(x,t) = \int_{-\infty}^{\infty} w(y) \int_0^{\infty} \eta(s) \sum_{m\in\mathbb{Z}} \delta(s - t + T^m(x-y))\mathrm{d}s\mathrm{d}y. \tag{2}$$

This models the effect of an idealized action potential (delta-Dirac function) arriving at a synapse and initiating a postsynaptic current $\eta(t - T^m)$ at time $T^m$. The convolution over space takes into account the connectivity pattern of the synapses between neurons. For simplicity it is assumed to be isotropic and homogeneous. If the synaptic response is on a slower time scale than that of the mean interspike-interval $(T^m - T^{m-1})$, and fluctuations around the mean are small, then it is natural to replace the spike train in (2) with a (smooth) firing rate function of synaptic activity (see for example [18]). This firing rate function is prescribed purely in terms of the properties of the single neuron model (1).

Firing rate models are expected to be valid for synaptic responses sufficiently slow so that the single neuron feels an effectively constant input over some long time-scale. For a given firing rate function of synaptic current, $f(u)$, synaptic dynamics is therefore determined by the integral equation

$$u(x,t) = \int_{-\infty}^{\infty} w(y) \int_{0}^{\infty} \eta(s) f(u(x-y, t-s)) \mathrm{d}s \mathrm{d}y. \tag{3}$$

There are a number of firing rate functions that may be derived from biophysical models. As discussed by Ermentrout [19], there are basically three ways in which a model can switch from silence to repetitive firing: (i) Hopf bifurcation, (ii) saddle-node on a limit cycle bifurcation, and (iii) global homoclinic bifurcation. In the sub-critical Hopf case, the oscillations appear with a finite frequency that is bounded away from zero. The appearance of repetitive firing at a nonzero frequency is rare in models of cortex (see [20]). More typical of cortical models is that the firing rate appears at a zero frequency via one of the two other mechanisms, (ii) or (iii). When repetitive activity is generated via a saddle-node bifurcation on an invariant circle the firing rate function behaves as $\sqrt{u-u_c}$. When a homoclinic bifurcation underlies the rhythmic behavior then the firing rate follows $[\ln(u/(u-u_c))]^{-1}$. In fact such a functional form is easy to derive for the often studied integrate-and-fire model [18]. In both cases $u = u_c$ is interpreted as the bifurcation point.

Typically, as the (constant) current, $u$ is increased, most cortical neurons switch from a resting constant potential to an active mode. In the active mode, either trains of spikes are generated or burst of spikes. Since the majority of cells in cortical networks fire repetitively [21], we shall focus our attention on this case. A common choice for the firing rate function is the sigmoid

$$f(u) = (1 + \exp(-\beta(u-h)))^{-1}, \tag{4}$$

which satisfies the Ricatti equation $\mathrm{d}f/\mathrm{d}u = \beta f(1-f)$ and saturates to one for large $u$. This functional form, with threshold $h$ and steepness parameter $\beta$, is not derived from a biophysical model, rather it is seen as a reasonable fit to experimental data.

Spatio-temporal delays arising from the finite conduction velocities of action potentials mean that the firing rate model (3) should be modified to

$$u(x,t) = \int_{-\infty}^{\infty} w(x-y) \int_{-\infty}^{t} \eta(t-s) f(u(y, s-|x-y|/v)) \mathrm{d}s \mathrm{d}y. \tag{5}$$

Here $v$ represents the velocity of action potential propagation and for simplicity we ne-

glect the possibility of a distribution of velocities. In the absence of any space-dependent delays, i.e. $v \to \infty$, it has been shown by Ermentrout and McLeod that there exists a unique monotone traveling wave front for sigmoidal firing rate functions and positive spatially decaying weight functions [22]. The effects of space-dependent delays have largely been dropped from the mathematical analysis of neural field equations. Note, however, that there is some work by Schumacher on asymptotic wave speed estimates, in the presence of space dependent delays, valid for the case that $\eta(t) \to \delta(t)$ [23]. In light of the mathematical difficulties associated with the introduction of space dependent delays, it is beneficial to first explore a re-formulation of the integral model (5) in terms of a partial differential equation.

## 3 PDE reduction

We shall consider symmetric synaptic footprints with $w(x) = w(|x|)$ and normalized synapses such that $\int_0^\infty \eta(t)\mathrm{d}t = 1$. It is convenient to use the language of Green's functions and write

$$Q\eta(t) = \delta(t), \tag{6}$$

where $\eta(t)$ is the Green's function of some linear differential operator $Q$, with $\eta(t) = 0$ for $t \leq 0$. Two common choices of synaptic kernel are the exponential function:

$$\eta(t) = \alpha \mathrm{e}^{-\alpha t}, \qquad Q = 1 + \alpha^{-1}\partial_t, \tag{7}$$

and the alpha function

$$\eta(t) = \alpha^2 t \mathrm{e}^{-\alpha t}, \qquad Q = (1 + \alpha^{-1}\partial_t)^2, \tag{8}$$

where $\alpha > 0$. After applying $Q$ to both sides of (5), we then have

$$Qu(x,t) = \psi(x,t), \qquad \psi(x,t) = \int_{-\infty}^{\infty} w(x-y) f(u(y, t-|x-y|/v))\mathrm{d}y. \tag{9}$$

The function $\psi(x,t)$ may be expressed in the form

$$\psi(x,t) = \int_{-\infty}^{\infty} \mathrm{d}y \int_{-\infty}^{\infty} G(x-y, t-s)\rho(y,s)\mathrm{d}s, \tag{10}$$

where

$$G(x,t) = \delta(t - |x|/v)w(x) \tag{11}$$

can be interpreted as another type of Green's function, and we use the notation

$$\rho(x,t) = f(u(x,t)). \tag{12}$$

Introducing Fourier transforms of the following form

$$\psi(x,t) = \frac{1}{(2\pi)^2}\int_{-\infty}^{\infty}\int_{-\infty}^{\infty} \mathrm{e}^{-\mathrm{i}(kx+\omega t)}\psi(k,\omega)\mathrm{d}k\mathrm{d}\omega, \tag{13}$$

allows us to write

$$\psi(k,\omega) = G(k,\omega)\rho(k,\omega), \tag{14}$$

assuming the Fourier transform of $f(u)$ exists. It is straightforward to show that the Fourier transform of (11) is

$$G(k,\omega) = \nu(\omega/v + k) + \nu(\omega/v - k), \tag{15}$$

where

$$\nu(E) = \int_0^{\infty} w(x)\mathrm{e}^{-\mathrm{i}Ex}\mathrm{d}x. \tag{16}$$

For now we shall focus on two different, yet common, forms of (normalized) synaptic footprint. The exponential synaptic footprint is given by

$$w(x) = \exp(-|x|/\sigma)/2\sigma, \qquad \nu(E) = \frac{1}{2\sigma}\frac{1}{\sigma^{-1} + \mathrm{i}E}, \tag{17}$$

whilst the square footprint is given by

$$w(x) = \Theta(\sigma - |x|)/2\sigma, \qquad \nu(E) = \frac{1}{2\sigma}\frac{\mathrm{i}}{E}[\mathrm{e}^{-\mathrm{i}\sigma E} - 1], \tag{18}$$

where $\sigma > 0$. Here $\Theta(x)$ represents the Heaviside step function. It is natural to exploit the product structure of (14) and properties of (15) to re-formulate the original integral model in terms of a partial differential equation. For the exponential synaptic footprint, we have using (15) and (17) that

$$G(k,\omega) = \frac{1 + \mathrm{i}\frac{\omega}{\omega_0}}{\left(1 + \mathrm{i}\frac{\omega}{\omega_0}\right)^2 + \sigma^2 k^2}, \tag{19}$$

where $\omega_0 = v/\sigma$. We may now write (14) as

$$\left\{\left(1 + \mathrm{i}\frac{\omega}{\omega_0}\right)^2 + \sigma^2 k^2\right\}\psi(k,\omega) = \left(1 + \mathrm{i}\frac{\omega}{\omega_0}\right)\rho(k,\omega), \tag{20}$$

which upon inverse Fourier transforming gives the PDE:

$$\psi_{tt} + \left(\omega_0^2 - v^2\partial_{xx}\right)\psi + 2\omega_0\psi_t = \left(\omega_0^2 + \omega_0\partial_t\right)\rho. \tag{21}$$

This is a type of damped wave equation with an inhomogeneity dependent on (12). This equation has previously been derived by Jirsa and Haken [17] and studied intensively in respect to the brain-behavior experiments of Kelso *et al.* [24]. Interestingly, the same approach applied to the case of the synaptic footprint with compact support yields a very different type of PDE. Using (15) and (18) gives

$$G(k,\omega) = \frac{1}{2\sigma}\frac{ie^{-i\omega/\omega_0}}{k^2 - \omega^2/v^2}\left[\left(\frac{\omega}{v}\right)\left[e^{i\sigma k} + e^{-i\sigma k} - 2e^{i\omega/\omega_0}\right] + k[e^{i\sigma k} - e^{-i\sigma k}]\right]. \tag{22}$$

Hence, we may obtain the following PDE for $\psi(x,t)$:

$$\begin{aligned} 2\sigma\left[\partial_{xx} - \frac{1}{v^2}\partial_{tt}\right]\psi(x,t) = \frac{1}{v}\partial_t[\rho(x+\sigma,t-\sigma/v) - 2\rho(x,t) + \rho(x-\sigma,t-\sigma/v)] \\ +\partial_x[\rho(x+\sigma,t-\sigma/v) - \rho(x-\sigma,t-\sigma/v)], \end{aligned} \tag{23}$$

which may be thought of as a non-local wave equation with retarded sources. This illustrates the fact that in general the basic model is non-local and that general choices of synaptic kernel may not lead to an equivalent local PDE representation. Techniques that would have been appropriate for studying (21), such as moving to a traveling wave frame and shooting for fronts, are obviously no longer appropriate. Apart from the challenge of analyzing solutions to (23) there is also the interesting question of how best to implement its numerical solution on a finite domain. In the next section we take a step in this direction and present results on traveling wave solutions to (21) and (23). These are obtained with a mixture of exact analysis for the special case that the firing rate function is a threshold function and numerical analysis of solutions to a set of traveling wave ODEs for sigmoidal firing rate functions given by (4).

## 4 Traveling waves

In light of the transformation of our original integral equation to a PDE we now have two complementary mathematical formulations in which we may construct traveling wave solutions. In both cases we assume solutions of the form $u(x,t) = u(x-ct)$. The original formulation still requires the direct solution of an integral equation, whilst the PDE description reduces to an ODE one. For sigmoidal firing rate functions it is natural to

look for traveling wave solutions with $u(-\infty) = 1$ and $u(\infty) = 0$. The solution for $u(\xi)$ is given by

$$u(\xi) = \int_0^\infty \eta(z)\psi(\xi + cz)\mathrm{d}z, \tag{24}$$

where the speed of the wave is determined by the *phase* condition $u(0) = h$. Of course this requires knowledge of the function $\psi(\xi)$. In general the wave equations for $\psi(\xi)$ must be solved in conjunction with the dynamics for $u(\xi)$. When the synaptic footprint is of the exponential type the function $\psi$ satisfies the following ODE

$$(c^2 - v^2)\psi_{\xi\xi} - 2\omega_0 c\psi_\xi + \omega_0^2\psi = (\omega_0^2 - c\omega_0\partial_\xi)\rho. \tag{25}$$

When the synaptic footprint has a square footprint then

$$2\sigma\left(\frac{c^2}{v^2} - 1\right)\psi_{\xi\xi}(\xi) = \mu_-\rho_\xi(\xi + \sigma\mu_+) - 2\mu_0\rho_\xi(\xi) + \mu_+\rho_\xi(\xi + \sigma\mu_-), \tag{26}$$

where $\mu_0 = c/v$. This is a delayed ODE where the delays are both advanced and retarded. The analysis of mixed functional differential equations is quite complicated and even the basic existence-uniqueness theory has not been established [25]. For the special case that $\rho_\xi$ is a linear function of $u$ and $c = 0$ the resulting differential-difference equation belongs to a class recently discussed by Elmer and Van Vleck [26]. It is possible that a generalization of their numerical solution scheme may be appropriate for exploring solutions to the system of equations defined by (26), (24) and the condition $u(0) = h$. However, it is also possible to make immediate and exact progress for both types of synaptic footprint with a choice of firing rate function that we shall now introduce.

### *4.1 Exact solutions*

In the limit $\beta \to \infty$ the firing rate function (4) approaches a Heaviside step function with a threshold at $u = h$. In this case we may solve the wave equations explicitly since $\psi$ depends only on the value of the threshold and not the shape of $u$. This observation was originally made by Pinto and Ermentrout [10]. We exploit their techniques to analyze in detail various forms of synaptic processing and connectivity.

For the case of an exponential synaptic footprint the solution to (25) is given in terms of a linear combination of exponentials with exponents $m_\pm\xi$ (and a constant for $\xi < 0$), where

$$m_\pm = \frac{\omega_0}{c \pm v}. \tag{27}$$

For the determination of the speed of the wave we only need a solution for $\xi > 0$. If we restrict ourselves to the physiological regime $|c| < v$, so that wave speeds cannot exceed conduction velocity, then for $\psi$ to be bounded as $\xi \to \infty$ requires

$$\psi(\xi) = A\exp(m_-\xi), \qquad \xi > 0. \tag{28}$$

From (9) we have that

$$\psi(\xi) = \int_{-\infty}^{\infty} w(y) f(u(\xi - y + c|y|/v))\mathrm{d}y, \tag{29}$$

with $\psi(0) = 1/2$, so that we must choose $A = 1/2$. Continuity of the solution at $\xi = 0$ and boundedness for $\xi \to -\infty$ means that for $\xi < 0$, $\psi(\xi) = 1 - \exp(m_+\xi)/2$. Hence, using $u(0) = h$, the speed of a wave with an exponential synaptic footprint and exponential synapse is given by

$$2h = [1 - cm_-/\alpha]^{-1} \quad \text{or} \quad c = \frac{v(2h-1)}{2h - 1 - 2hv/(\alpha\sigma)}. \tag{30}$$

It is easily seen that the speed of the wave is zero when $h = 1/2$. For the other case with a square footprint we use the fact that $\rho_\xi(\xi) = \partial_\xi\Theta(\xi) = \delta(\xi)$ to see that the right hand side of (26) causes jumps in $\psi_\xi$ of size $1/2\sigma\mu_-$, $-\mu_0/\sigma\mu_+\mu_-$ and $1/2\sigma\mu_+$ at $\xi = -\sigma\mu_-$, $\xi = 0$ and $\xi = -\sigma\mu_+$ respectively. A piecewise linear solution that connects $\psi = 0$ and $\psi = 1$ with $\psi(0) = 1/2$ is therefore given by

$$\psi(\xi) = \begin{cases} 1 & \xi \le -\sigma\mu_+ \\ \frac{1}{2}\left(1 - \frac{\xi}{\sigma\mu_+}\right) & -\sigma\mu_+ < \xi \le 0 \\ \frac{1}{2}\left(1 + \frac{\xi}{\sigma\mu_-}\right) & 0 < \xi < -\sigma\mu_- \\ 0 & \xi \ge -\sigma\mu_- \end{cases}. \tag{31}$$

Using the phase condition $u(0) = h$ we find that the speed of the wave with a square synaptic footprint and exponential synapse is given implicitly by

$$2h - 1 = \frac{1}{\gamma(c)}\left[1 - \exp\gamma(c)\right], \qquad \gamma(c) = \sigma\mu_-\alpha/c. \tag{32}$$

Once again we see that $c = 0$ when $h = 1/2$.

The wave speed for an alpha function synapse may be calculated in an analogous fashion. We have respectively for the exponential and square footprint that the speed of a wave

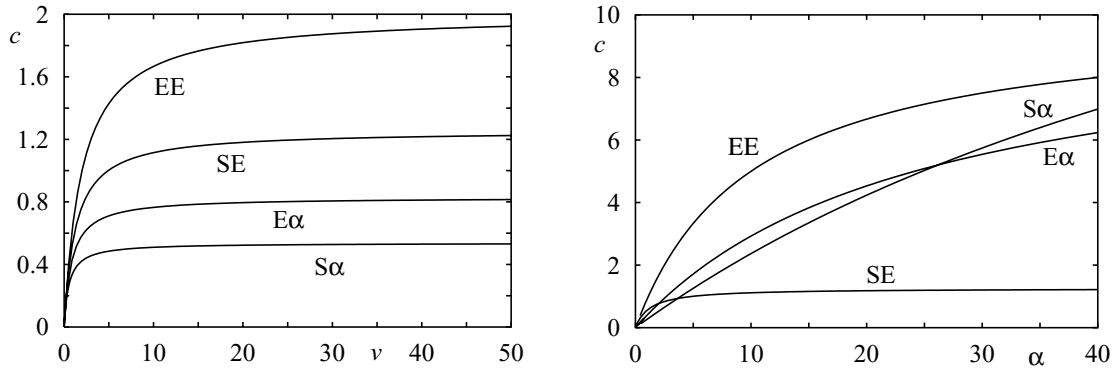


Fig. 1. Wave speed in the limit of infinite gain (Heaviside firing rate function), as a function of $v$ (left, with $\alpha = 2$) and $\alpha$ (right, with $v = 10$). In both cases, $\sigma = 1$ and $h = 1/4$. EE: exponential footprint and exponential synapse, E$\alpha$: exponential footprint and alpha synapse, SE: square footprint and exponential synapse, S$\alpha$: Square footprint and alpha synapse.

---

(with an alpha synapse) is given by

$$2h = [1 - cm_-/\alpha]^{-2} \tag{33}$$

$$2h - 1 = \frac{2}{\gamma(c)}\left[1 - \exp\gamma(c)\right] + \exp\gamma(c). \tag{34}$$

In both cases the speed of the wave vanishes when $h = 1/2$. It is easy to establish that for small $v$ the wave speed, for all our choices of footprint and synapse, is controlled by the conduction velocity of the action potential so that $c \sim v$. A plot of wave speeds as a function of system parameters is shown in Figure 1.

### *4.2 Numerical solutions*

Here we explore the effect of finite $\beta$ on the behavior of traveling fronts when the synaptic footprint is exponential. In this case we may analyze solutions in the traveling wave frame using standard numerical techniques, such as shooting. For an exponential synapse we have a 3D system of equations defined by (7), (24), (25), and for an alpha synapse we have a 4D system defined by (8), (24), (25). To construct traveling wave fronts we look for bounded orbits that are heteroclinic connections to the rest states in the traveling wave frame. We implemented in Auto97 [27] the projection boundary conditions of [28]. We truncate and rescale the traveling wave coordinate to the interval $[0, 1]$ and project out the stable and unstable manifolds at $\xi = 0$ and $\xi = 1$. After imposing an integral phase condition

it is then possible to perform numerical continuation of solutions in system parameters. Initial data for the traveling wave boundary value problem was obtained using successive continuation [29]. Projection boundary conditions are more accurate than a large fixed period periodic approximation since the error due to truncation to a finite interval is exponentially small [28, 30].

Figure 2 shows plots of wave speed against $\beta$ for both cases. Note that there are three homogeneous steady states, $u_1 < u_2 < u_3$, and the upper branch corresponds to waves connecting $u_3$ to $u_2$ (not expected to be realizable in neural systems, since $u_2$ is unstable) and the lower to waves connecting $u_3$ to $u_1$. The limit point at the left of the bifurcation diagram (Figure 2) corresponds to a fold bifurcation in the local dynamics, where the $u_2$ and $u_1$ steady states are lost.

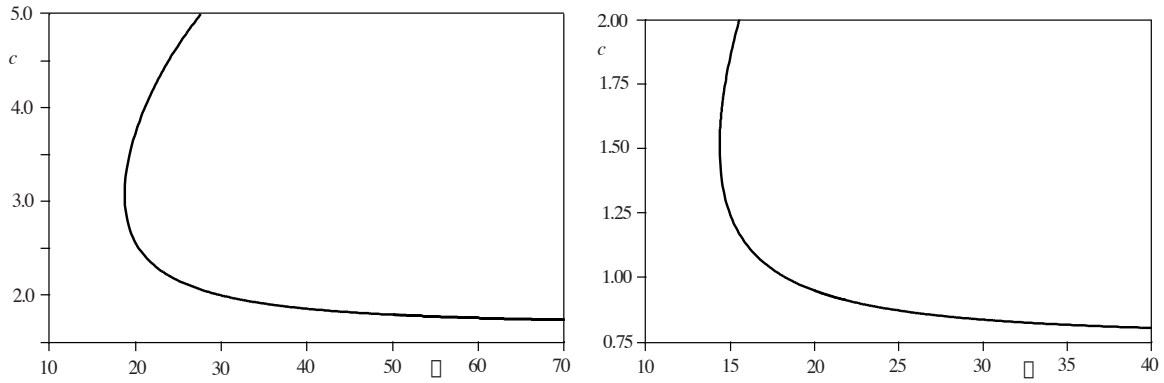


Fig. 2. Bifurcation diagram showing wave speed against $\beta$ for: (Left) the traveling wave speed for the 3D system (7), (24), (25); (Right) wave speed for the 4D system (8), (24), (25). The limit points at the left correspond to the loss of two homogeneous steady states through a fold bifurcation. The lower branch corresponds to waves connecting locally stable fixed points, and the upper branch to those connecting locally stable to unstable fixed points. This correspondence mirrors that for other bistable systems. Parameter values are $h = 0.25, \sigma = 1, \alpha = 2, v = 10$.

## 5 Spike frequency adaptation

In real cortical tissues there are an abundance of metabolic processes whose combined effect is to modulate neuronal response. It is convenient to think of these processes in terms of local feedback mechanisms that modulate synaptic currents. It is likely that such feedback will modify behavior in the wake of a traveling front so as to bring activity back

down to some resting level. Here we consider a simple model of so-called *spike frequency adaptation* (SFA) that can lead to the formation of propagating pulses. For a detailed discussion of biophysical models for SFA in networks of spiking neurons see, for example, the work of Liu and Wang [31]. An additional phenomenological current is included on the right hand side of (9), so that

$$Qu(x,t) = \psi(x,t) - ga(x,t), \qquad \frac{\partial a(x,t)}{\partial t} = -a + \kappa f(u(x,t)), \tag{35}$$

where $g, \kappa > 0$. A similar form has been studied previously, for the case of exponential synapses, infinite conduction velocities, and with the $a$ equation linear in $u$ [10]. The nonlinearity considered here allows for exact analysis in the limit of infinite gain, including the effects of space dependent delays.

Since $\psi(x,t)$ is given as before it only remains to determine the shape and speed of a traveling pulse of the form $u(\xi_1) = u(\xi_2) = h$, $u(\xi) \geq h$ for $\xi_1 < \xi < \xi_2$ and $\lim_{\xi\to\pm\infty} u(\xi) = 0$. We shall denote the difference $\xi_2 - \xi_1 > 0$ by $\Delta$. Boundary conditions may then be used to determine the pulse speed.

For illustrative purposes we follow through this program to give an exact traveling pulse solution for the case of an exponential synaptic footprint, an exponential synapse and $\beta \to \infty$. The dynamics for $a$ may be solved as

$$a(\xi) = \begin{cases} \kappa[1 - \mathrm{e}^{-\Delta/c}]\,\mathrm{e}^{(\xi-\xi_1)/c} & \xi \leq \xi_1 \\ \kappa[1 - \mathrm{e}^{(\xi-\xi_2)/c}] & \xi_1 < \xi < \xi_2 \\ 0 & \xi \geq \xi_2 \end{cases}. \tag{36}$$

In the limit $\beta \to \infty$ the function $\psi(\xi)$ may be conveniently written using (29) as

$$\psi(\xi) = \begin{cases} \mathcal{F}\left(\frac{\xi_1-\xi}{c/v+1}, \frac{\xi_2-\xi}{c/v+1}\right) & \xi \leq \xi_1 \\ \mathcal{F}\left(0, \frac{\xi_1-\xi}{c/v-1}\right) + \mathcal{F}\left(0, \frac{\xi_2-\xi}{c/v+1}\right) & \xi_1 < \xi < \xi_2 \\ \mathcal{F}\left(\frac{\xi_2-\xi}{c/v-1}, \frac{\xi_1-\xi}{c/v-1}\right) & \xi \geq \xi_2 \end{cases}, \tag{37}$$

where

$$\mathcal{F}(a,b) = \int_a^b w(y)\mathrm{d}y. \tag{38}$$

Hence, for an exponential synaptic footprint the solution is

$$\psi(\xi) = \begin{cases} \frac{1}{2}(\mathrm{e}^{m_+(\xi-\xi_1)} - \mathrm{e}^{m_+(\xi-\xi_2)}) & \xi \le \xi_1 \\ 1 - \frac{1}{2}(\mathrm{e}^{m_+(\xi-\xi_2)} + \mathrm{e}^{m_-(\xi-\xi_1)}) & \xi_1 < \xi < \xi_2 \\ \frac{1}{2}(\mathrm{e}^{m_-(\xi-\xi_2)} - \mathrm{e}^{m_-(\xi-\xi_1)}) & \xi \ge \xi_2 \end{cases}. \tag{39}$$

Thus, for an exponential synapse the solution for $u(\xi)$ is

$$u(\xi) = \frac{\alpha}{c}\int_{\xi}^{\infty} \mathrm{e}^{\alpha(\xi-z)/c}[\psi(z) - ga(z)]\mathrm{d}z.$$

It just remains to enforce the conditions $u(\xi_{1,2}) = h$, giving the two equations

$$h[1-\mathrm{e}^{-\alpha\Delta/c}] = (1-\mathrm{e}^{-\alpha\Delta/c})(1-g\kappa) + \frac{1}{2}\left\{\frac{\mathrm{e}^{-\alpha\Delta/c} - \mathrm{e}^{-m_+\Delta}}{1-cm_+/\alpha} + \frac{\mathrm{e}^{(m_- - \alpha/c)\Delta} - 1}{1-cm_-/\alpha}\right\} + \alpha g\kappa\frac{\mathrm{e}^{-\Delta/c} - \mathrm{e}^{-\alpha\Delta/c}}{\alpha - 1} \tag{40}$$

$$h = \frac{1}{2}\frac{1-\mathrm{e}^{m_-\Delta}}{1-cm_-/\alpha}. \tag{41}$$

The simultaneous solution of (40) and (41) determines the dispersion relation $c = c(h, v, \alpha, g, \kappa)$. Figure 3 shows the pulse speed and width as $\kappa$ varies, with stable pulses corresponding to the upper branch (based upon the evidence of extensive numerical simulations). We find that the wave speed is not markedly different to that of fronts. Taking the limit $\Delta \to \infty$ in (40) and (41) and adding the two equations together shows that in this limit $2h = 1 - gk$. Hence, wide pulses (large $\Delta$) fail to propagate if $\kappa < \kappa_c$, where

$$\kappa_c = \frac{1-2h}{g}. \tag{42}$$

Thus in Figure 3 the width of pulse solutions diverges to infinity as $\kappa \to \kappa_c$. Direct numerical simulations suggest that it is the faster of the two possible branches that is stable. Hence, when $\kappa < \kappa_c$ only stable traveling fronts are expected. In Figure 4 we continue the limit point of Figure 3 where $\kappa = \kappa_{\mathrm{sn}}$, at which pulses are destroyed with increasing $\kappa$, in the $(\kappa, h)$ and $(\kappa, v)$ parameter planes. It is clear that stable pulses are only possible in the parameter regime where $\kappa_c < \kappa < \kappa_{\mathrm{sn}}$. As the threshold $h$ is reduced, or the conduction velocity $v$ is increased, the range of $\kappa$ which allows pulse solutions increases. Figure 5 illustrates a numerically simulated pulse solution with finite conduction velocities that closely agrees with our exact calculation. The evolution equation (35) was solved by discretizing space and using the ODE solver `ode45` in MATLAB to evolve the resulting

space-dependent delayed differential equation. To increase the speed of computation, space and time convolutions were calculated using fast Fourier transforms.

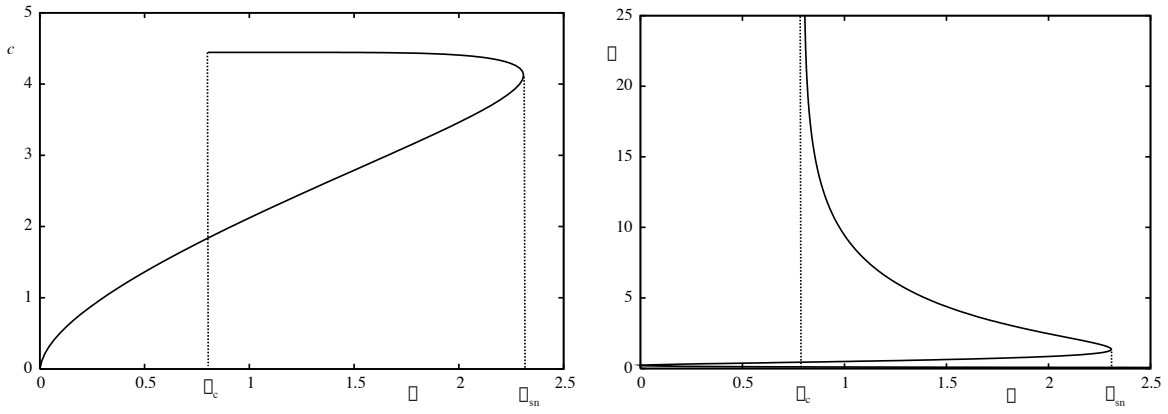


Fig. 3. Wave speed and width for traveling pulse solutions with $g = 1, h = 0.1, \alpha = 2, \sigma = 1$ and $v = 10$. Note that numerical simulations indicate that stable pulses correspond to the upper branch, and hence that there is a minimum pulse width. For large $\Delta$, when $\kappa \to \kappa_c$ from above, the speed of the pulse is approximately that of the front.

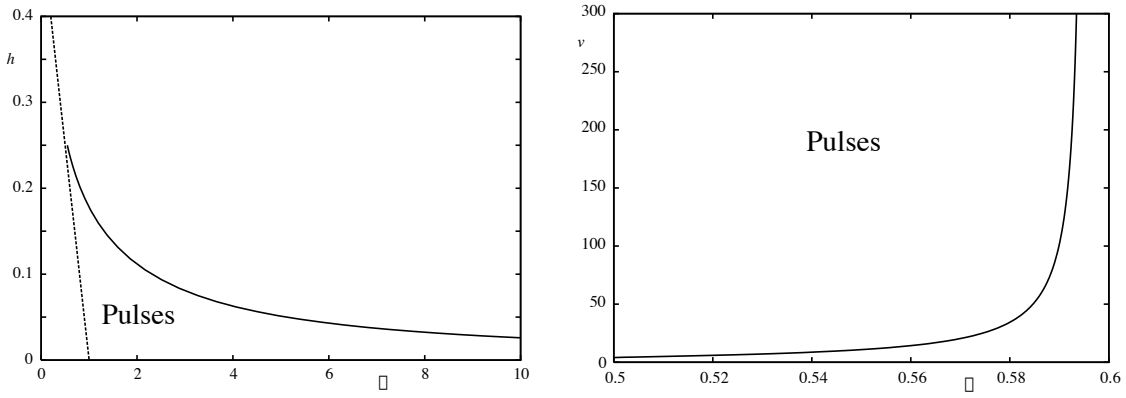


Fig. 4. Ranges in $(\kappa, h)$ (with $v = 10$) and $(\kappa, v)$ (with $h = 0.25$) space which allow pulses, with other parameters as in Figure 3.

## 6 Dendritic interactions

In our discussion so far we have completely ignored the influence of the dendritic tree on network dynamics. Dendrites are large branched structures, attached to a neuronal cell body (soma), upon which incoming fibres make synaptic connections. At the very least,

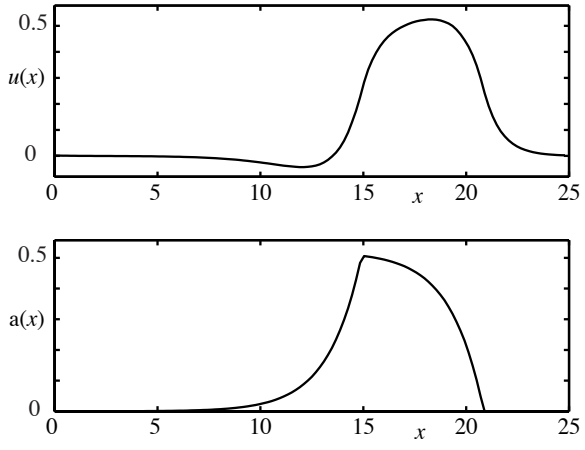


Fig. 5. Numerically simulated traveling pulse solution with $g = 1$,$h = 0.25$, $\alpha = 2$, $\sigma = 1$, $\kappa = 0.52$ and $v = 10$. The predicted pulse speed and width are $c = 1.664$ and $\Delta = 5.7991$ respectively, compared to values from the simulation of $c = 1.62$ and $\Delta = 5.94$. Numerical simulations used the MATLAB ode solver `ode45` together with fast Fourier transforms for the calculation of convolutions. Space dependent delays mean that the convolution is two-dimensional, limiting the resolution in this simulation to a $128 \times 128$ spatio-temporal grid.

---

they act as a spatio-temporal filter for patterns of incoming activity. This means that the somatic response depends both on (i) previous input history (due to the existence of distributed delays arising from voltage diffusion throughout a dendritic tree), and (ii) the particular locations of the stimulated synapses on the tree (i.e. the distribution of axo-dendritic connections). In this section we broaden our discussion to include the effects of biologically realistic choices of axo-dendritic interactions in networks with simple unbranched electrically passive dendrites. In particular we are interested in the observation that a synapse tends to be located further away from the soma or cell body as the separation between neurons increases. Previous work by Bressloff [32] has already established that such patterns of axo-dendritic connectivity can give rise to a Turing-like instability, leading to the formation of stable spatial and time-periodic patterns of network activity. For the moment, we wish to focus on the nature of traveling wave solutions in such networks. Necessarily we must generalize equation (1) to include the effects of a simple model dendrite. We shall take as our model dendrite the standard one dimensional unbranched uniform cable equation, with voltage $U(x, X, t)$ at position $X \geq 0$ along a semi-infinite cable with somatic coordinate $x$:

$$U_t = -\frac{U}{\tau} + DU_{XX} + I(x, X, t). \tag{43}$$

Here, $\tau$ is recognized as the membrane time-constant of the dendrite, $D$ as the cable diffusion coefficient and $I(x, X, t)$ is the synaptic input:

$$I(x, X, t) = \int_{-\infty}^{t} \eta(t - s)\mathrm{d}s \int_{-\infty}^{\infty} W(X, x - y) f(u(y, s - |x - y|/v))\mathrm{d}y. \tag{44}$$

Thus $I(x, X, t)$ is a convolution over the spatial extent of the network (i.e. over somatic coordinates), together with a convolution over time representing synaptic processing. The distribution and strength of axo-dendritic connections is specified by the choice of $W(X, |x|)$, and we assume that an axonal connection from a neuron at $y$ to the dendrite of a neuron at $x$ has a length which scales linearly with the distance between neurons, so that axonal delays are given by $|x-y|/v$. Note that we allow the strength of synaptic connections to vary, but we assume the temporal responses of all synapses are the same. For convenience we consider the soma to be at position $X = 0$. At the end of the dendritic cable adjoining the soma we impose the boundary condition $\partial V(x, X, t)/\partial X|_{X=0} = 0$. Note that this assumes that the feedback from the soma to the dendrite can be neglected [33]. If the soma is resistively coupled to the end of the dendrite at $X = 0$ then we have that $u(x, t) = \rho[U(x, 0, t) - V(x, t)]$, for some constant conductance $\rho$. If we then consider the derivation of a firing rate model as in section 2 we find that the conductance $\rho$ leads to a modification of the firing rate function and that it is natural to consider simply $u(x, t) = \rho U(x, 0, t)$. Hereafter, we shall set $\rho = 1$ without loss of generality. The linearity of (43) means that we may use the Green's function of the cable equation, $G(X, t)$, associated with the linear differential operator $Q = \partial_t + \tau^{-1} - D\partial_{XX}$, to write

$$u(x, t) = \int_{-\infty}^{t} \mathrm{d}s \int_{0}^{\infty} \mathrm{d}Y G(Y, t - s) I(Y, x, s). \tag{45}$$

To model cortical anatomy in a biologically plausible fashion we choose the distribution

$$W(X, x) = \frac{1}{2}\delta(X - |x|), \tag{46}$$

which incorporates the fact that synapses are located further away from the soma as the separation between neurons increases. The factor of two is merely chosen for convenience (and would be dropped if we had chosen an infinite rather than semi-infinite cable). If we also consider instantaneous synapses of the form $\eta(t) = \delta(t)$, and infinite conduction velocities, then (45) is recognized as the solution to the reaction-diffusion equation

$$u_t = -\frac{u}{\tau} + Du_{xx} + f(u). \tag{47}$$

For sigmoidal firing rate functions, (47) may have three homogeneous steady states ($u_1 < u_2 < u_3$), and will exhibit typical behavior for such so-called *cubic kinetics* [34]. Traveling waves connecting $u_1$ and $u_3$ (which are stable to homogeneous perturbations) will predominate, and will propagate in directions determined by the sign of $\int_{u_1}^{u_3}[f(u) - u/\tau]\mathrm{d}u$ [35]. Waves connecting to the unstable intermediate state $u_2$ do exist, but are always such that $u_1$ or $u_3$ propagate into regions at $u_2$. Thus we would only see such waves persist in neural systems if the initial conditions were at $u_2$ everywhere except for the initial disturbance, and such initial conditions would be highly unlikely due to the instability of $u_2$.

For the case that $f(u) = \Theta(u - h)$, $u_3$ only exists if $h < \tau$, and in the traveling wave frame we may write the solution to (47) in the form

$$u(\xi) = \begin{cases} \tau + A \exp \lambda_+(c)\xi & \xi \leq 0 \\ B \exp \lambda_-(c)\xi & \xi > 0 \end{cases}, \tag{48}$$

where

$$\lambda_\pm(c) = \frac{-c \pm \sqrt{c^2 + 4D/\tau}}{2D}. \tag{49}$$

Continuity of the solution and its first derivative at $\xi = 0$ determines $A$ and $B$ as

$$A = \frac{\tau\lambda_-(c)}{\lambda_-(c) - \lambda_+(c)}, \qquad B = \frac{\tau\lambda_+(c)}{\lambda_-(c) - \lambda_+(c)} \tag{50}$$

The speed of the wave is then specified by the constraint $u(0) = h$, which gives

$$c = \sqrt{D}\frac{\frac{1}{h} - \frac{2}{\tau}}{\sqrt{\frac{1}{h} - \frac{1}{\tau}}}, \qquad h < \tau. \tag{51}$$

Hence the speed of the wave scales as $\sqrt{D}$ and changes direction when $h = \tau/2$. If $h > \tau$, the firing threshold is too high to sustain activity, and waves do not propagate.

In Figure 6 we present a numerical analysis, using the same techniques as in earlier Sections, showing how these results extend to smooth sigmoidal firing rate functions (4). Note that as $\beta$ decreases, the firing rate function becomes less steep, and the pair of steady states $u_1$ and $u_2$ approach each other. Thus, the left most point in the figure corresponds to a fold bifurcation at which the two states, and consequently traveling waves, are lost.

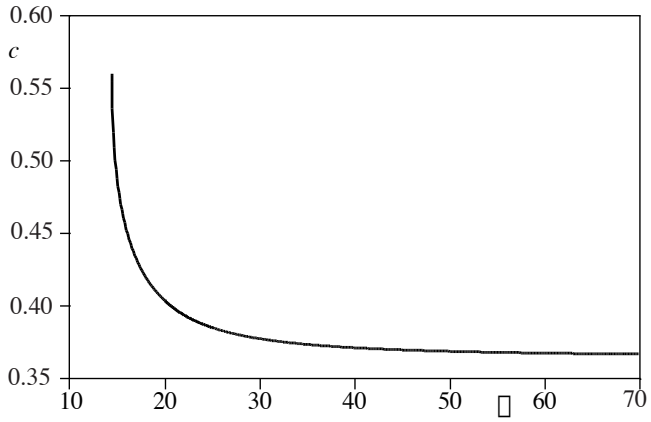


Fig. 6. Wave speed for (47) as a function of $\beta$, which measures the steepness of the firing rate function (4). Parameters are $h = 0.25$, $D = 0.1$, and $\tau = 1$.

## 7 Static patterns

### *7.1 From dendrites to Mexican hats*

We consider equation (45) under the assumption that the dendritic cable instantaneously equilibriates (small dendritic membrane capacitance), which is equivalent to replacing $\int_{-\infty}^{t} \mathrm{d}s G(Y, t-s) I(Y, x, s)$ in (45) with $\widehat{G}(Y) I(Y, x, t)$, where $\widehat{G}(Y) = \int_0^\infty \mathrm{d}s G(Y, s)$, so that

$$u(x,t) = \int_0^\infty \mathrm{d}Y \widehat{G}(Y) \int_{-\infty}^{t} \mathrm{d}s \eta(t-s) \int_{-\infty}^{\infty} \mathrm{d}y W(Y, x-y) f(u(y, s-|x-y|/v)). \qquad (52)$$

Introducing the Laplace transform $\widetilde{G}(x, E) = \int_0^\infty G(x,t) \mathrm{e}^{-Et} \mathrm{d}t$, allows us to write $\widehat{G}(Y) = \widetilde{G}(Y, 0)$. The Laplace transform of $G(x,t)$ is well known (see for example [36]), and it is a simple matter to check that

$$\widehat{G}(X) = \frac{\mathrm{e}^{-\nu|X|}}{2D\nu}, \qquad \nu^2 = \frac{1}{\tau D}. \qquad (53)$$

Now if we consider a distribution of synaptic connections whose distance from the soma increases linearly with the distance between neurons, and that the strength of synaptic response decreases linearly with that distance, we have $W(X, x) = \delta(X - |x|)(w_0 - w_1|X|)$. Combining the above reduction of the cable Green's function and this anatomical

description gives an equation of the form (5) with

$$w(x) = \frac{1}{2D\nu}(w_0 - w_1|x|)\mathrm{e}^{-\nu|x|}, \qquad w_0,\ w_1 > 0. \tag{54}$$

Hence, we see how the inclusion of axo-dendritic interactions can provide a mechanism for generating effective connectivities of Mexican hat shape. It is well known that (without the effects of space-dependent delays) models like (5) support localized patterns when $w(x)$ is a Mexican hat function.

### *7.2 Exact homoclinic solution*

Here we construct static (time-independent) patterns of the form $u(x,t) = u(x)$ for all $t$ where $Qu(x) = u(x)$. Using (5) gives

$$u(x) = \int_{-\infty}^{\infty} w(x-y)f(u(y))\mathrm{d}y. \tag{55}$$

Based upon the arguments above, we shall assume the synaptic kernel has a Mexican hat shape given by

$$w(x) = \frac{w_0}{4}(1 - |x|)\mathrm{e}^{-|x|}. \tag{56}$$

We consider the limit $\beta \to \infty$ and look for solutions of the form $\lim_{x\to\pm\infty} u(x) = 0$, with $u(x) \geq h$ for $x_1 < x < x_2$. In this case the exact solution is given simply by

$$q(x) = \int_{x_1}^{x_2} w(x-y)\mathrm{d}y. \tag{57}$$

For the Mexican hat function (56), a simple calculation gives

$$\frac{4}{w_0}q(x) = \begin{cases} g(x-x_1) - g(x-x_2) & x > x_2 \\ g(x_2-x) + g(x-x_1) & x_1 \leq x \leq x_2\ , \\ g(x_2-x) - g(x_1-x) & x < x_1 \end{cases} \tag{58}$$

where $g(x) = x\mathrm{e}^{-x}$. The conditions $q(x_1) = h$ and $q(x_2) = h$ both lead to the equation

$$w_0\Delta\mathrm{e}^{-\Delta} = 4h, \tag{59}$$

describing a family of solutions with $\Delta = (x_2 - x_1)$. Hence, homoclinic bumps are only possible if $4h/w_0 < 1/\mathrm{e}$. The full branch of solutions for $\Delta = \Delta(h)$ is shown in Figure 7.

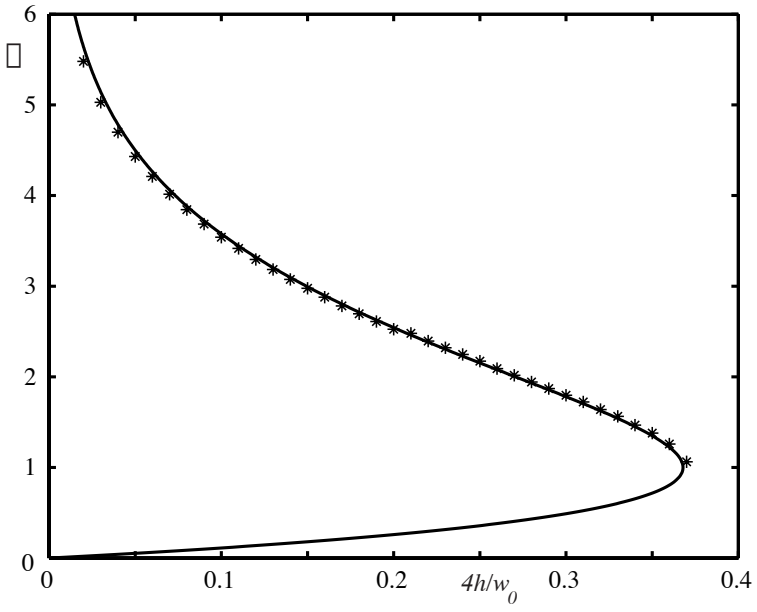


Fig. 7. Bump width as a function of $4h/w_0$, as determined by equation (59) for a step function firing rate function and Mexican hat kernel (56). Asterisks indicate bump width for numerical simulations (using MATLAB `ode45` plus fast Fourier transforms for convolutions).

---

One of the translationally invariant solutions may be picked by imposing a *phase* condition $q(0) = q_0$, where $q_0 \leq \max q(x) = w_0 \Delta \mathrm{e}^{-\Delta/2}/4$ (which occurs at $(x_1 + x_2)/2$ using (58)). An example is illustrated in Figure 8.

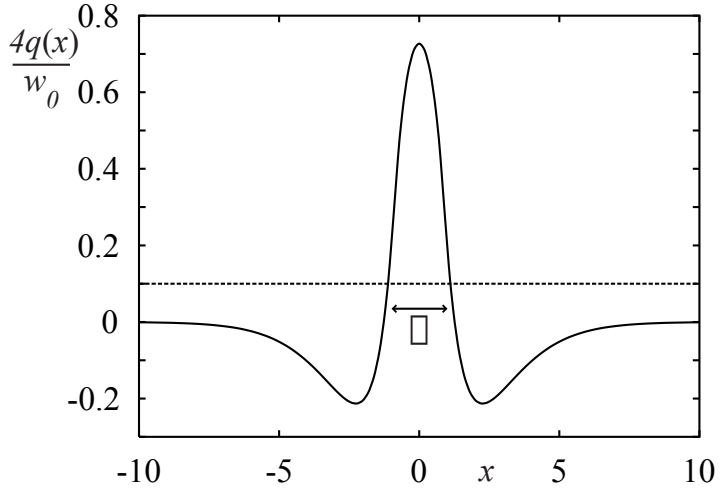


Fig. 8. An example of a stable homoclinic bump with $4h/w_0 = 0.1$.

---

It is also possible to construct $P$ periodic solutions, $r(x) = r(x+P)$, in a similar fashion, with the result $r(x) = \sum_{n\in\mathbb{Z}} q(x+nP)$. The dispersion curve $\Delta = \Delta(P)$ is obtained by ensuring $r(x_i) = h$ [16].

### *7.3 An equivalent fourth order ODE*

Recent work by Laing *et al.* [11] has established a link between fourth order Hamiltonian equations and the non-local integral equations that arise naturally in neural field theories. Motivated by their work we present the associated Hamiltonian system for (55) when the synaptic footprint is the Mexican hat given by (56). This particular synaptic footprint has a nice integral representation given by

$$w(x) = w_0 \int_{-\infty}^{\infty} \frac{\mathrm{d}k}{2\pi} \frac{k^2}{(1+k^2)^2} \mathrm{e}^{-\mathrm{i}kx}, \tag{60}$$

which may be verified by choosing contours in the upper ($x > 0$) and lower ($x < 0$) complex half-plane. To obtain an ODE corresponding to (55) it is natural to once again make use of Fourier transforms. In this way we find that an equivalent ODE to (55) is

$$(1 - \mathrm{d}_{xx})^2 u = -w_0 [f(u)]_{xx}. \tag{61}$$

This fourth order ODE is reversible (since only even derivatives of $u$ occur) and has a first integral of the form

$$-\frac{1}{2}(u_{xx})^2 + u_x u_{xxx} - (u_x)^2 + \int_0^u [s + g(s)]\mathrm{d}s, \tag{62}$$

where $g(u) = w_0[f(u)]_{xx}$. In fact (61) has a Hamiltonian structure (see Appendix), although we shall not make use of that here. Note that high order reversible Hamiltonian equations are intimately related to pattern formation in physical systems. We refer in particular to the models reviewed by Cross and Hohenberg [37] and Champneys [38].

In order to study this system we approximate global homoclinic connections by computing solutions on a fixed (large) interval, using similar techniques as for computing traveling waves in earlier sections, but making explicit use of the reversible structure. Figure 9 shows the $L_2$ norm of solutions for (61), as the threshold $h$ varies. For this parameter regime we see a pair of disconnected snaking curves, one tracing $N$-bumps with $N$ odd and the other with $N$ even. Such bifurcation diagrams are characteristic of the existence of a connection between the fixed point and a periodic, as observed previously in mechanical

structure problems (see [39, 40, 41]). Each pass around the left fold of the *snake* introduces another bump on either side of the original solution. These sorts of snaking curves were first observed in a neural context by Laing *et al.* [11]. In this paper the authors found that, for a Heaviside firing rate function, multi-bumps are only possible if the synaptic connectivity is oscillatory and spatially decaying. Our results show that multi-bumps are possible even for simple Mexican-hat connectivity functions (without oscillatory decay) as long as the firing rate function is sigmoidal. Direct numerical simulations suggest that for a given pair of $N$ bump solutions it is the one with largest $L_2$ norm that is stable. The evolution of such solutions in the full time-dependent system (5) is illustrated in Figure 10.

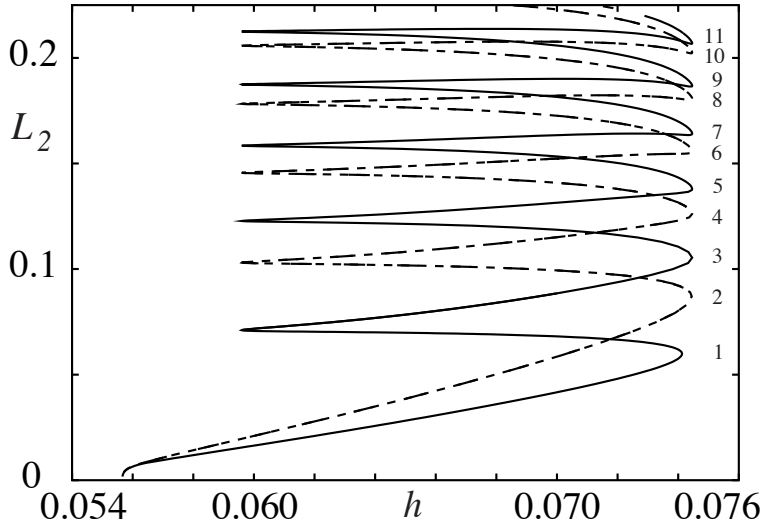


Fig. 9. Continuation in $h$ for the 4th order ODE (61). Parameter values are $\beta = 30$ and $w_0 = 1$. The solid (dashed) line shows the locus of $N$-bump solutions for $N$ odd (even). Numbers on the right hand side refer to the number of bumps in a solution. Note that all $N$-bump solutions occur in pairs and it is the one with largest $L_2$ norm that is stable.

---

### *7.4 Stability*

For zero axonal delays ($v \to \infty$) and $\beta \to \infty$ the stability of bumps may be investigated using the techniques of Amari [16]. We use the threshold condition $u(x_i, t) = h$ to define the locations $x_{1,2}$ from which we obtain the equations of motion of the boundary as

$$\frac{\mathrm{d}x_i}{\mathrm{d}t} = -\frac{\frac{\partial u}{\partial t}}{\frac{\partial u}{\partial x_i}}. \tag{63}$$

It is then possible to calculate the rate of change of the interval $\Delta(t) = x_2(t) - x_1(t)$ using

$$u_t(x,t) = \eta(0)\int_{x_1(t)}^{x_2(t)} w(x-y)\mathrm{d}y + \int_{-\infty}^{t}\eta'(t-s)\int_{x_1(s)}^{x_2(s)} w(x-y)\mathrm{d}s\mathrm{d}y. \tag{64}$$

For example, with $\eta(t) = \alpha\exp(-\alpha t)$, then (for a single bump)

$$\frac{\mathrm{d}\Delta}{\mathrm{d}t} = \alpha\left(\frac{1}{c_1}+\frac{1}{c_2}\right)[q(x_1)-h], \tag{65}$$

where

$$c_1 = \frac{\partial u(x_1,t)}{\partial x}, \qquad -c_2 = \frac{\partial u(x_2,t)}{\partial x}. \tag{66}$$

Hence, the equilibrium solution defined by $u(x_1) = h$ is stable if

$$\frac{\mathrm{d}q(x_1)}{\mathrm{d}\Delta} = w(\Delta) < 0. \tag{67}$$

In our previous example $w(\Delta) = w_0\exp(-\Delta)(1-\Delta)/4$, so that of the two possible branches of $\Delta = \Delta(h)$, it is the one with largest $\Delta$ that is stable.

Since there is no obvious way in which to generalize the stability approach of Amari to cover the case of space dependent delays we develop a more general linear stability analysis. This can be accomplished by examining the eigenspectrum of the linearization about a solution. Assuming the solutions of the linearized system to have the form $u(x)\,\mathrm{e}^{\lambda t}$ leads naturally to the eigenvalue problem $\mathcal{L}u(x) = u(x)$, where

$$\mathcal{L}u(x) = \int_{-\infty}^{\infty} w(x-y)\,\mathrm{e}^{-\lambda|x-y|/v}\int_0^{\infty}\eta(s)\,\mathrm{e}^{-\lambda s}\,f'(q(y))u(y)\mathrm{d}s\mathrm{d}y. \tag{68}$$

The eigenfunction associated with the eigenvalue $\lambda = 0$ (arising from translation symmetry) is $q'(x)$, but the extraction of other eigenfunctions can probably only be done numerically. However, for the case of a Heaviside firing rate function we can again make explicit progress using the result

$$\int_{-\infty}^{\infty}\mathrm{d}x f'(q(x))F(x) = \int_{-\infty}^{\infty}\mathrm{d}x\delta(q(x)-h)F(x) = \int_{-\infty}^{\infty}\frac{\mathrm{d}z}{|q'(q^{-1}(z))|}\delta(z-h)F(q^{-1}(z)). \tag{69}$$

Using the further result that $q'(x) = w(x-x_1) - w(x-x_2)$ and remembering that $q(x_{1,2}) = h$ the eigenvalue equation reduces to

$$u(x) = \frac{\widetilde{\eta}(\lambda)}{|w(0)-w(\Delta)|}[w(x-x_1)u(x_1)\,\mathrm{e}^{-\lambda|x-x_1|/v} + w(x-x_2)u(x_2)\,\mathrm{e}^{-\lambda|x-x_2|/v}], \tag{70}$$

where $\widetilde{\eta}(\lambda) = \int_0^{\infty}\eta(s)\,\mathrm{e}^{-\lambda s}\,\mathrm{d}s$. The equality in (70) implies that if $u(x_{1,2}) = 0$ then $u(x) = 0$ for all $x$. Following [12] we now examine the matrix equation obtained from (70)

at the points $x = x_{1,2}$,

$$\begin{bmatrix} u(x_1) \\ u(x_2) \end{bmatrix} = \frac{\widetilde{\eta}(\lambda)}{|w(0) - w(\Delta)|} \begin{bmatrix} w(0) & w(\Delta)\,\mathrm{e}^{-\lambda|\Delta|/v} \\ w(\Delta)\,\mathrm{e}^{-\lambda|\Delta|/v} & w(0) \end{bmatrix} \begin{bmatrix} u(x_1) \\ u(x_2) \end{bmatrix}. \tag{71}$$

Non-trivial solutions are only possible if

$$\frac{1}{\widetilde{\eta}(\lambda)} = \frac{w(0) \pm w(\Delta)\,\mathrm{e}^{-\lambda|\Delta|/v}}{|w(0) - w(\Delta)|}. \tag{72}$$

Solutions will be stable if $\mathrm{Re}(\lambda) < 0$. It is a simple matter to check that there is always one solution with $\lambda = 0$. For an exponential synapse $\widetilde{\eta}(\lambda) = (1 + \lambda/\alpha)^{-1}$ and we see that as $v \to \infty$ solutions are only stable if $(w(0) + w(\Delta))/|w(0) - w(\Delta)| < 1$. Noting that this is true if $w(\Delta) < 0$ we recover the result of Amari, as expected. In the other extreme where $v \to 0$ it is simple to show that real and positive values for $\lambda$ can only occur when $w(\Delta) > 0$. Hence, as $v$ is varied there are no new instabilities due to real eigenvalues passing through zero. However, for finite conduction velocities it is possible that solutions may destabilize via a Hopf bifurcation. By writing $\lambda = \mathrm{i}\omega$ the conditions for a Hopf bifurcation, where $\mathrm{Re}(\lambda) = 0$ and $\mathrm{Im}(\lambda) \neq 0$, are obtained from the simultaneous solution of

$$1 = \frac{w(0) + w(\Delta)\cos(\omega|\Delta|/v)}{|w(0) - w(\Delta)|}, \qquad \frac{\omega}{\alpha} = -\frac{w(\Delta)\sin(\omega|\Delta|/v)}{|w(0) - w(\Delta)|}. \tag{73}$$

Eliminating $\sin(\omega|\Delta|/v)$ between these two equations gives

$$\omega^2 = \frac{\alpha^2}{|w(0) - w(\Delta)|^2}\left[w^2(\Delta) - \{|w(0) - w(\Delta)| - w(0)\}^2\right]. \tag{74}$$

The condition that $\omega \neq 0$ requires the choice $w(\Delta) > w(0)$, which does not hold for (56). Hence, the presence of space dependent delays neither affects the existence or stability of bump solutions.

### *7.5 Numerical simulations*

Numerical simulations of the integral model (5), with the Mexican hat kernel (56), illustrate the exact single bump solutions derived above. Figure 7 includes bump widths calculated by evolving the time dependent system—these simulations were carried out in the absence of space-dependent delays to enable rapid calculations to a high degree of

accuracy (2048 spatial grid points were used). Further simulations with finite conduction velocities used two-dimensional convolutions in space and time, and fully supported the above analysis of bump stability.

More importantly, Figure 10 demonstrates that multiple bump solutions are possible for finite $\beta$. Further calculations show that a localized bump is destabilized to a global pattern as the threshold $h$ is reduced (Figure 11). These observations are in agreement with the bifurcation analysis of the 4th order ODE system (61), whose solutions are steady states of the integral model. In Figure 9 the branches correspond to multi-bump solutions of the kind shown in Figure 10, while the folds at the left of Figure 9 correspond to the loss of localized bump solutions to global patterns (indicated in Figure 11).

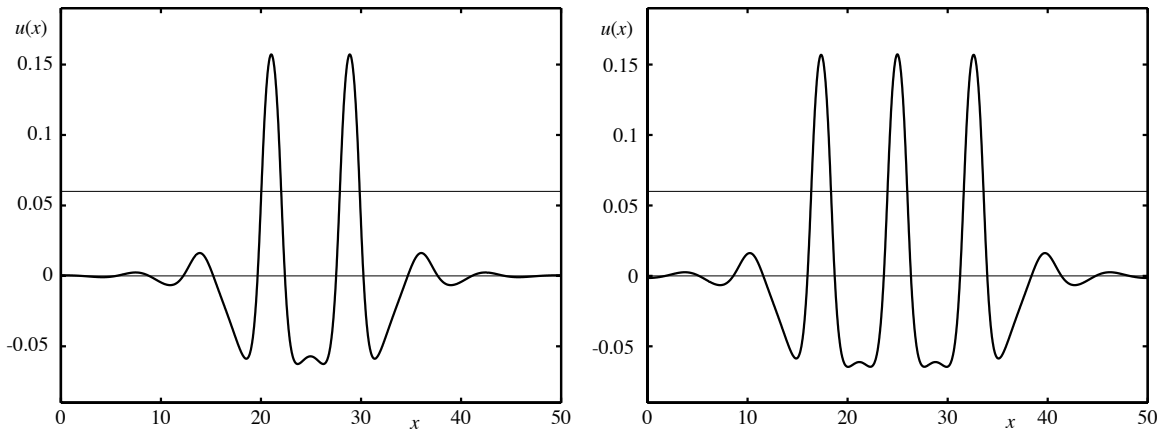


Fig. 10. Localized solutions with multiple bumps are possible, with the number of peaks selected by initial conditions. The parameter values were $\beta = 30, \alpha = 2, w_0 = 1$ and $h = 0.06$. The threshold $h$ is indicated by the upper horizontal line.

---

In the limit of infinite gain it has been shown analytically that 2-bumps can only exist close together, and furthermore such 2-bumps are thought to be unstable [11]. Our simulations support this instability of close peaks. However, pairs of bumps do arise in numerical simulations and move apart extremely slowly, so much so that they appear stable. This can be understood by considering the pair of equations which would determine the equal widths, $\Delta$, and separation between peaks, $s$, of 2-bumps:

$$\Delta \mathrm{e}^{-\Delta} - s\mathrm{e}^{-s} + (s+\Delta)\mathrm{e}^{-(s+\Delta)} = \frac{4h}{w_0}, \quad \Delta \mathrm{e}^{-\Delta} + s\mathrm{e}^{-s} - (s-\Delta)\mathrm{e}^{-s+\Delta} = \frac{4h}{w_0}. \qquad (75)$$

As $s \to \infty$ we recover the condition for a single bump solution (59), and it turns out that both conditions may rapidly asymptote to the width of an isolated single bump. Thus

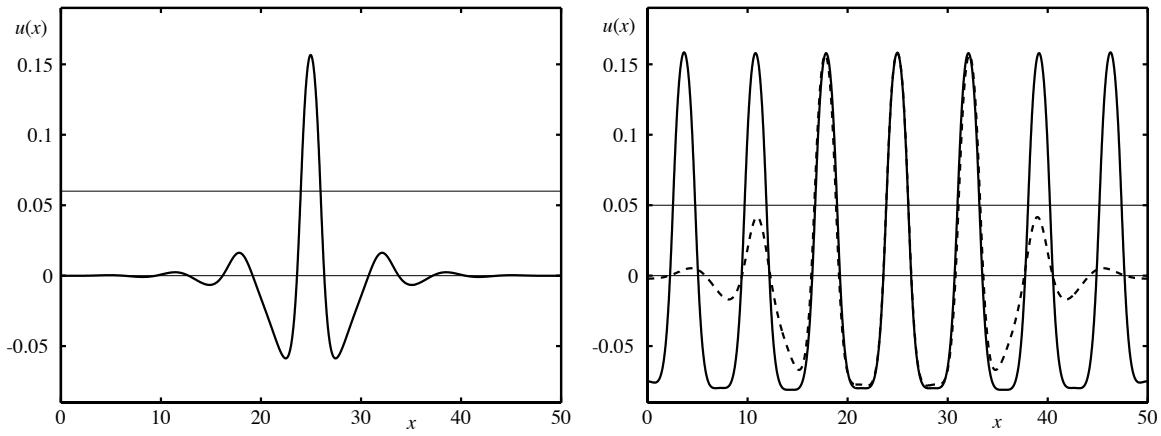


Fig. 11. Numerical simulations of the integral model (5), with the Mexican hat kernel given by (56), show that a localized bump is destabilized to a global pattern. The parameter values were $\beta = 30, \alpha = 2, w_0 = 1$ and $h = 0.06$ and $h = 0.05$ respectively. In the latter case the solution is shown as it evolves to a global pattern. The dashed line is the solution at $t = 10$ and the solid line is the solution at $t = 40$.

---

even for finite $s$ both conditions are very nearly satisfied, and the rate of separation of a pair of peaks rapidly falls below the limit of numerical round-off. Intuitively, this is simply a property of the decay of the Mexican hat kernel—if bumps are sufficiently far apart, they do not "see" each other. Since for infinite gain it is only the regions above threshold that interact, solutions need not even decay to zero between peaks.

## 8 Discussion

In this paper we have incorporated axo-dendritic synaptic processing and axonal delays into neural field theories of Wilson-Cowan type. We have discussed the transformation of this revised integral model to an equivalent PDE model and highlighted the fact that this does not always simplify further mathematical analysis. In particular, for weight kernels with compact support, the equivalent PDE model requires advanced and retarded terms and questions of existence and uniqueness remain open. Nonetheless, in a traveling wave frame, we have constructed exact solutions for the case that the firing rate function is a Heaviside step function. This has also provided a self-consistent manner in which to test the success of numerical construction and continuation of solutions. A simple model of spike frequency adaptation was shown to alter traveling wave solutions from fronts to pulses, without strongly affecting wave speed. For passive dendritic trees and biologically

realistic choices of axo-dendritic synaptic connectivities we have shown that wave speed scales with the diffusion coefficient of the dendrite and that waves will fail to propagate if the firing rate threshold is too large. In common with many other studies of neural field theories we find that synaptic connectivities with Mexican hat profile give rise to spatial patterns of activity. We have shown that this is to be expected since there is an equivalent fourth order Hamiltonian system for the time-independent solution of the integral model. However, as recently pointed out by Swindale [42], it is surprisingly difficult to find physiological and anatomical data to support the case of short-range excitation and long-range inhibition assumed in standard models of neural pattern formation. Importantly we have shown that the inclusion of passive dendrites obviates the need for a Mexican hat connectivity, assuming that synaptic density increases at distal dendritic locations and changes from excitatory to inhibitory moving away from the soma.

There are a number of natural ways in which to extend the work presented. From a mathematical perspective, traveling front and pulse solutions are not structurally stable so that the introduction of even small inhomogeneities in the connectivity pattern may lead to propagation failure. Motivated by the anisotropic and inhomogeneous nature of many cortical areas it should be possible, using averaging and homogenization theory, to uncover the role of the periodic microstructure of cortex in front and pulse propagation and its failure, along the lines developed in [43].

The analysis of the spectrum of $\mathcal{L}$ (and its counterpart for traveling waves) for general firing rate functions is an important open problem. Of special interest are the conditions for the de-stabilization of a static bump in favor of a traveling wave. It is worth noting that some results on the asymptotic stability of traveling waves in integro-differential equations, of the form considered in this paper, have recently been obtained by Terman and Zhang using geometric singular perturbation theory [44].

It is also important to remember that in specific brain regions, such as mammalian neocortex, connectivity patterns follow a laminar arrangement, with strong vertical coupling between layers. Consequently cortical activity is considered as occurring on a two-dimensional plane, with the coupling between layers ensuring near instantaneous vertical propagation. Apart from recent work by Taylor [45] and Werner and Richter [46] planar studies have received relatively little attention. The two dimensional generalization of our work will open up the challenge to understand the effects of axo-dendritic synapses and axonal communication delays on spiral waves and target patterns.

Much of the analytical progress has been made under the assumption that dendrites behave linearly. However, there has long been evidence that nonlinear membrane properties are not confined to the axon hillock, but are spread throughout the dendritic tree [47]. The techniques of this paper can be easily extended to cover so-called quasi-active membrane (linearized Hodgkin-Huxley kinetics) that is thought relevant to understanding experimentally observed sub-threshold voltage oscillations associated with voltage-dependent ionic channels distributed along the dendritic tree [48]. In contrast to the purely passive model of a dendritic tree the Green's function of the model tree will have an oscillatory component reflecting more closely the band-pass nature of real dendritic tissue. The inclusion of recently observed excitable channels capable of generating action potentials [49] is a much harder challenge.

Finally, let us not forget that the firing rate description of neural tissue is likely to break down for fast synaptic responses. In this case one must resort to the study of spiking models where synaptic currents are given by expressions like (2). These studies are highly non-trivial, although some progress has been made in finding the conditions for a Turing-Hopf instability leading to the formation of periodic patterns in oscillatory networks [18, 50] and the conditions for obtaining localized bistable bumps in excitable networks [51].

## Acknowledgments

We would like to thank Carlo Laing, Bill Troy, Bard Ermentrout and Tony Humphries for helpful comments made during the completion of this paper.

SC and GJL would like to acknowledge support from the London Mathematical Society.

## Appendix

Equation (61) can be formulated as a Hamiltonian system. Define $v = u'$, $p_u = -2u' + u'''$ and $p_v = -u''$. The Hamiltonian in these new variables is

$$H(u, v, p_u, p_v) = -\frac{1}{2}p_v^2 + vp_u + v^2 + \int_0^u [s + g(s)]\mathrm{d}s, \tag{76}$$

and (61) is equivalent to the Hamiltonian system

$$\begin{aligned} u' &= \frac{\partial H}{\partial p_u}, \qquad & p_u' &= -\frac{\partial H}{\partial u} \\ v' &= \frac{\partial H}{\partial p_v}, \qquad & p_v' &= -\frac{\partial H}{\partial v}. \end{aligned} \tag{77}$$

## References


[1] D Golomb and Y Amitai. Propagating neuronal discharges in neocortical slices: Computational and experimental study. *Journal of Neurophysiology*, 78:1199–1211, 1997.

[2] R Miles, R D Traub, and R K S Wong. Spread of synchronous firing in longitudinal slices from the CA3 region of hippocampus. *Journal of Neurophysiology*, 60:1481–1496, 1995.

[3] U Kim, T Bal, and D A McCormick. Spindle waves are propagating synchronized oscillations in the ferret LGNd *in vitro*. *Journal of Neurophysiology*, 74:1301–1323, 1995.

[4] Alan Roberts. How does a nervous system produce behaviour? A case study in neurobiology. *Science Progress Oxford*, 74:31–51, 1990.

[5] B W Connors and Y Amitai. Generation of epileptiform discharges by local circuits in neocortex. In P A Schwartzkroin, editor, *Epilepsy: Models, Mechanisms and Concepts*, pages 388–424. Cambridge University Press, 1993.

[6] C M Gray. Synchronous oscillations in neuronal systems: mechanisms and functions. *Journal of Computational Neuroscience*, 1:11–38, 1992.

[7] C L Colby, J R Duhamel, and M E Goldberg. Oculocentric spatial representation in parietal cortex. *Cerebral Cortex*, 5:470–481, 1995.

[8] D Golomb, X J Wang, and J Rinzel. Propagation of spindle waves in a thalamic slice model. *Journal of Neurophysiology*, 75:750–769, 1996.

[9] J Rinzel, D Terman, X J Wang, and B Ermentrout. Propagating activity patterns in large-scale inhibitory neuronal networks. *Science*, 279:1351–1355, 1998.

[10] D J Pinto and G B Ermentrout. Spatially structured activity in synaptically coupled neuronal networks: I. Travelling fonts and pulses. *SIAM Journal on Applied Mathematics*, 62:206–225, 2001.

[11] C R Laing, W C Troy, B Gutkin, and G B Ermentrout. Multiple bumps in a neuronal model of working memory. *SIAM Journal on Applied Maths (submitted)*, 2001.

[12] D J Pinto and G B Ermentrout. Spatially structured activity in synaptically coupled neuronal networks: II. Lateral inhibition and standing pulses. *SIAM Journal on Applied Mathematics*, 62:226–243, 2001.

[13] J Huguenard and D A McCormick. *Electrophysiology of the Neuron*. Oxford University Press, 1996.

[14] H R Wilson and J D Cowan. A mathematical theory of the functional dynamics of cortical and thalamic nervous tissue. *Kybernetik*, 13:55–80, 1973.

[15] P L Nunez. The brain wave equation: A model for the EEG. *Mathematical Biosciences*, 21:279–, 1974.

[16] S Amari. Dynamics of pattern formation in lateral-inhibition type neural fields. *Biological Cybernetics*, 27:77–87, 1977.

[17] V K Jirsa and H Haken. Field theory of electromagnetic brain activity. *Physical Review Letters*, 77:960–963, 1996.

[18] P C Bressloff and S Coombes. Dynamics of strongly-coupled spiking neurons. *Neural Computation*, 12:91–129, 2000.

[19] G B Ermentrout. Neural nets as spatio-temporal pattern forming systems. *Reports on Progress in Physics*, 61:353–430, 1998.

[20] J Rinzel and G B Ermentrout. Analysis of neural excitability and oscillations. In C Koch and I Segev, editors, *Methods in Neuronal Modeling*, pages 135–170. MIT Press, Cambridge MA, 1989.

[21] E L White. *Cortical Circuits: Synaptic Organization of the Cerebral Cortex. Structure, Function, and Theory*. Birkhauser, 1989.

[22] G B Ermentrout and J B McLeod. Existence and uniqueness of travelling waves for a neural network. *Proceedings of the Royal Society of Edinburgh*, 123A:461–478, 1993.

[23] K Schumacher. Travelling-front solutions for integrodifferential equations II. In W Jäger, H Rost, and P Tautu, editors, *Lecture Notes in Biomathematics: Biological Growth and Spread*, volume 38. Springer-Verlag, 1980.

[24] J A S Kelso, S L Bressler, S Buchanan, G C Deguzman, M Ding, A Fuchs, and T Holroyd. A phase-transition in human brain and behaviour. *Physics Letters A*, 169:134–144, 1992.

[25] J Wu and X Zou. Asymptotic and periodic boundary value problems of mixed FDEs and wave solutions of lattice differential equations. *Journal of differential equations*, 135:315–357, 1997.

[26] C E Elmer and E S Van Vleck. Analysis and computation of travelling wave solutions

of bistable differential-difference equations. *Nonlinearity*, 12:771–798, 1999.

[27] E J Doedel, A R Champneys, T R Fairgrieve, Y A Kuznetsov, B Sandstede, and X J Wang. AUTO97 continuation and bifurcation software for ordinary differential equations. 1997. Available from http://indy.cs.concordia.ca/auto/main.html.

[28] W J Beyn. The numerical computation of connecting orbits in dynamical systems. *IMA Journal of Numerical Analysis*, 9:379–405, 1990.

[29] E Doedel, M J Friedman, and B I Kunin. Successive continuation for locating connecting orbits. *Numerical Algorithms*, 14:103–124, 1997.

[30] B Sandstede. Convergence estimates for the numerical approximation of homoclinic solutions. *IMA Journal of Numerical Analysis*, 17:437–462, 1997.

[31] Y H Liu and X J Wang. Spike-frequency adaptation of a generalized leaky integrate-and-fire model neuron. *Journal of Computational Neuroscience*, pages 25–45, 2001.

[32] P C Bressloff. New mechanism for neural pattern formation. *Physical Review Letters*, 76:4644–4647, 1996.

[33] P C Bressloff. Dynamics of a compartmental model integrate-and-fire neuron with somatic potential reset. *Physica D*, 80:399–412, 1995.

[34] J D Murray. *Mathematical Biology*. Springer Verlag, Berlin, 1989.

[35] P C Fife. *Mathematical aspects of reacting and diffusing systems*. Springer Verlag, 1979.

[36] P C Bressloff and S Coombes. Physics of the extended neuron. *International Journal of Modern Physics B*, 11:2343–2392, 1997.

[37] M C Cross and P C Hohenberg. Pattern formation outside of equilibrium. *Reviews of Modern Physics*, 65:851–1112, 1993.

[38] A R Champneys. Homoclinic orbits in reversible systems and their applications in mechanics. *Physica D*, 112:158–186, 1998.

[39] P D Woods and A R Champneys. Heteroclinic tangles in the unfolding of a degenerate Hamiltonian Hopf bifurcation. *Physica D*, 129:147–170, 1999.

[40] G W Hunt, G J Lord, and A R Champneys. Homoclinic and heteroclinic orbits underlying the post-buckling of axially compressed cylindrical shells. *Computational Methods in Applied Mechanics Engineering, Special Issue Computational Methods and Bifurcation Theory*, 170:239–251, 1999.

[41] G W Hunt, M A Peletier, A R Champneys andP D Woods, M Ahmer Wadee, C J Budd, and G J Lord. Cellular buckling in long structures. *Nonlinear Dynamics, Theme issue on 'Localization'*, 21:3–29, 2000.

[42] N V Swindale. The development of topography in the visual cortex: A review of models. *Network*, 7:161–274, 1996.

[43] P C Bressloff. Traveling fronts and wave propagation failure in an inhomogeneous neural network. *Physica D*, 155:83–100, 2001.

[44] D Terman and L Zhang. Asymptotic stability of traveling wave solutions of integral-differential equations arising from neuronal networks. *preprint available from http://www.math.ohio-state.edu/∼terman/*, 2002.

[45] J G Taylor. Neural 'bubble' dynamics in two dimensions: foundations. *Biological Cybernetics*, 80:393–409, 1999.

[46] H Werner and T Richter. Circular stationary solutions in two-dimensional neural fields. *Biological Cybernetics*, 85:211–217, 2001.

[47] C Li and H H Jasper. Microelectrode studies of the electrical activity of the cerebral cortex in the cast. *Journal of Physiology*, 121:117–140, 1953.

[48] C Koch. Cable theory in neurons with active, linearized membranes. *Biological Cybernetics*, 50:15–33, 1984.

[49] I Segev and W Rall. Excitable dendrites and spines: earlier theoretical insights elucidate recent direct observations. *Trends in Neuroscience*, 21(11):453–460, 1998.

[50] P C Bressloff and S Coombes. Spike train dynamics underlying pattern formation in integrate-and-fire oscillator networks. *Physical Review Letters*, 81:2384–2387, 1998.

[51] C Laing and C C Chow. Stationary bumps in networks of spiking neurons. *Neural Computation*, 13:1473–1494, 2001.